



Atomic carbon chains-mediated carriers transfer over polymeric carbon nitride for efficient photocatalysis



Yunxiang Li^{a,b}, Jian Ren^{e,f}, Shuxin Ouyang^{c,d}, Weishu Hou^{c,d}, Tristan Petit^e, Hui Song^{a,b}, Huayu Chen^{c,d}, Davin Philo^{a,b}, Tetsuya Kako^b, Jinhua Ye^{a,b,c,d,*}

^a Graduate School of Chemical Sciences and Engineering, Hokkaido University, Sapporo, 060-0814, Japan

^b International Center for Materials Nanoarchitectonics (WPI-MANA), National Institute for Materials Science (NIMS), 1-1 Namiki, Tsukuba, 305-0044, Japan

^c TJU-NIMS International Collaboration Laboratory, School of Materials Science and Engineering, Tianjin University, Tianjin, 300072, PR China

^d Collaborative Innovation Center of Chemical Science and Engineering (Tianjin), Tianjin, 300072, PR China

^e Methods for Material Development, Helmholtz-Zentrum Berlin für Materialien und Energie GmbH (HZB), Albert-Einstein-Strasse 15, Berlin, 12489, Germany

^f Department of Physics, Freie Universität Berlin, Arnimallee 14, Berlin, 14195, Germany

ARTICLE INFO

Keywords:

Carbon nitride
Conductivity engineering
Carbon chains
Photocatalytic H₂ generation
CO₂ reduction

ABSTRACT

Atomic structure tailoring towards high electron mobility is an essential approach to maximizing the solar energy-conversion efficiency of polymeric carbon nitride (CN) but still presents a significant challenge. Here we construct a smooth carrier channel in the basal plane of CN by filling the rich defects in layer with various kinds of short carbon chains, whereby the light-induced carriers transfer kinetics is boosted distinctly. Consequently, the optimal carbon chains-planted CN delivers a remarkably enhanced photocatalytic performance, achieving a 13.2 and 29.2-fold improvement in H₂ evolution and CO₂ reduction, respectively. This study provides an in-depth insight into the modulation of in-plane electrical conductivity at molecular scale over CN and offers new opportunities for reinforcing the reaction kinetics of organic-based photocatalysts.

1. Introduction

The generation of clean and renewable chemicals from H₂O and CO₂ using photocatalysts is a highly promising solution to the conversion and storage of solar energy [1]. The development of efficient, durable, and sustainable photocatalysts is always at the heart of photocatalytic research. Layered polymeric carbon nitride (CN), a metal-free and chemically stable material, has attracted intense interest in all kinds of solar to chemical energy conversion process including H₂/O₂ evolution from water splitting and CO₂ reduction [2–11]. Owing to the unique chemical composition and layered feature, polymeric CN possesses high adjustability and compatibility and thus offer us huge potential to targetedly tailor its structure and properties towards diverse applications [12–21].

However, similar to other kinds of organic framework, e.g., metal-organic frameworks (MOFs), and covalent organic frameworks (COFs), efficient solar-to-energy conversion over polymeric CN still encounters great challenges of sluggish radiative carriers transfer within layers due to the long transportation distance and rich defects in layers. Notably, these defects in polymeric CN are mainly related to NH₂ and NH groups

because of the incomplete polymerization of amide groups-rich precursors [22]. Abundant intralayered hydrogen bonds are thus (as illustrated by the dash line in Scheme 1a) formed in the defect regions [22,23]. As a result, the transport of charge carriers across the layers of CN is signally different from that of other materials only containing covalent bonds within the layers, e.g., MoS₂ with Mo–S bonds and nitrogen doped graphene with C–N/C–C bonds [22]. These hydrogen bonds are not favorable relative to covalent bonds for the transport of photocarriers within the plane and thus cause the high localization of photocarriers within the tri-s-triazine units [22,24].

The direct atomic engineering of intralayered defects/motifs is the most fundamental and straightforward pathway to facilitate the transport of carriers in the layered CN and also can provide deeper insight into the behavior of the carriers in CN. Recently, several pioneering approaches have been sought in the perspective of this sight [13,25–27]. First, Liu et al. selectively broke the hydrogen bond via reducing the residual NH₂/NH groups at high temperature, in part resulting in a remarkable suppression of radiative carriers recombination in photocatalyst [22]. Another reported strategy is to implant the carbon ring including two similar types—“C_{ring}” and “gradually doped

* Corresponding author at: International Center for Materials Nanoarchitectonics (WPI-MANA), National Institute for Materials Science (NIMS), 1-1 Namiki, Tsukuba, 305-0044, Japan.

E-mail address: Jinhua.YE@nims.go.jp (J. Ye).

graphited carbon rings" into the planar layer of CN [25,26]. In the case of C_{ring} modified CN, the in-plane inserted C_{ring} not only expedites the carriers separation but also promotes the photoelectron transport [25]. Similarly, carbon quantum dots, with relatively larger size compared to atomic carbon ring, were also implanted in the 2D plane of CN seamlessly to facilitate the photoelectron transport [27]. However, these strategies above-mentioned still suffer from several drawbacks, such as moderate photocatalytic performance or complicated and energy consumption procedures. Besides, precise and targeted basal plane engineering of CN with atomic carbon species smaller than aforementioned carbon-based dopants, i.e., short carbon chains, has not been intentionally attempted yet and still remains a significant challenge.

Herein, we propose a conceptual and facile strategy to construct carbon chains incorporated CN, in which various kinds of carbon chains connected the in-plane defects of CN via strong covalent C–N bonds. Notably, these mediated carbon chains serve as the electron transport channel to reinforce the separation and transfer of photogenerated carriers in the basal plane of CN. Therefore, the optimized sample delivers a remarkably enhanced photocatalytic performance by achieving a 13.2 and 29.2-fold improvement for water reduction and CO_2 reduction, respectively, as well as good stability without noticeable attenuation.

2. Experimental

2.1. Materials preparation

All reagents were analytical grade and used without further purification. The deionized water (18.2 MΩ) that was used throughout all experiments was produced using a Millipore Direct-Q System. The pristine polymeric CN (denoted as CN) was fabricated by annealing 1.5 g melamine up to 550 °C at a rate of 2.3 °C min⁻¹ and kept for 4 h in a covered Al₂O₃ crucible. After cooled down to room temperature, the product was grounded to obtain a powder sample. To fabricate the carbon chains linked CN precursors (melamine/dicyandiamide/urea/thiourea) and linker molecules (glycine/β-Alanine/4-Aminobutyric acid/L-cysteine/Allyl thiourea/L-Arginine) were first mixed fully. Using the linker glycine as an example, 1.5 g melamine and certain amount of glycine (5, 10, 15, 20, 30 mg) were first dissolved in 20 mL deionized water with stirring and heated at ~80 °C to evaporate the water. Then, the white mixture followed the identical calcination procedure of CN as mentioned above. The samples thus obtained were named as CN-xGly, where x (mg) represents the amount of glycine. As shown in Fig. 3a,b, the optimized amount of glycine was 10 mg. Therefore, for other linkers, the amount was roughly fixed at 10 mg to evaluate the validity of different linkers on photocatalytic activity. Other carbon chains doped samples derived from various precursors, i.e., dicyandiamide/urea/thiourea, were fabricated following the similar procedures with that of CN-xGly but with different precursor and dosage. Specially, in the case of samples prepared from urea and thiourea, the amount of both of them is 10 g. The samples in Fig. 3d were fabricated using precursor dicyandiamide and different linker molecules. The CN-10Gly-(two steps) was synthesis by heating the mixture of CN (~600 mg, derived from 1.5 g melamine) and 10 mg glycine at 550 °C.

2.2. Physicochemical characterization

XRD patterns of the as-prepared samples were collected with a powder X-ray diffractometer (Cu Kα radiation source, X'pert powder, PANalytical B.V., Netherlands). UV-visible (UV-vis) diffuse reflectance spectra of the samples were recorded on an UV-visible spectrophotometer (UV-2700, Shimadzu, Japan) equipped with an integrating sphere, then converted into absorption spectra by Kubelka–Munk transformation. Nitrogen adsorption–desorption isotherms, and surface area were recorded using a BEL SORP-mini II (BEL Japan INC., Japan), and were calculated via the Brunauer–Emmett–

Teller (BET) method. Infrared transmission spectra were collected using a Fourier Transform infrared (FT-IR) spectrophotometer (Nicolet 4700, Thermo SCIENTIFIC, America). The in situ FT-IR measurements were conducted on a JASCO FTIR-6300 spectrometer under argon with a homemade chamber. The Photoluminescence (PL) properties were investigated using a fluorescence spectrophotometer (Fluorolog-3, HORIBA Scientific, America). X-ray photoelectron spectroscopy (XPS) measurements were carried out on XPS instrument (Escalab 250, Thermo SCIENTIFIC, America). All binding energies were referenced to the C 1 s peaks of the surface adventitious carbon at 284.8 eV. The morphologies of samples were characterized with Field Emission Scanning Electron Microscope (JSM-6701 F, JEOL Co., Japan) and Transmission Electron Microscope (TEM) (JEM-2100 F, JEOL Co., Japan). X-ray absorption spectroscopy measurements were carried on CN samples drop casted on conductive Si wafer. The data were collected at the U49/2 PGM1 undulator beamline of the BESSY II synchrotron radiation source using the LiXEldrom endstation. The XAS were measured in the total electron yield mode by scanning the samples in the energy range of 276–310 eV (for C K-edge) or 395–420 eV (for N K-edge) in 0.1 eV steps. The XAS spectra in the figures have been normalized to the background before and after the main features.

2.3. Photocatalytic H_2 evolution test

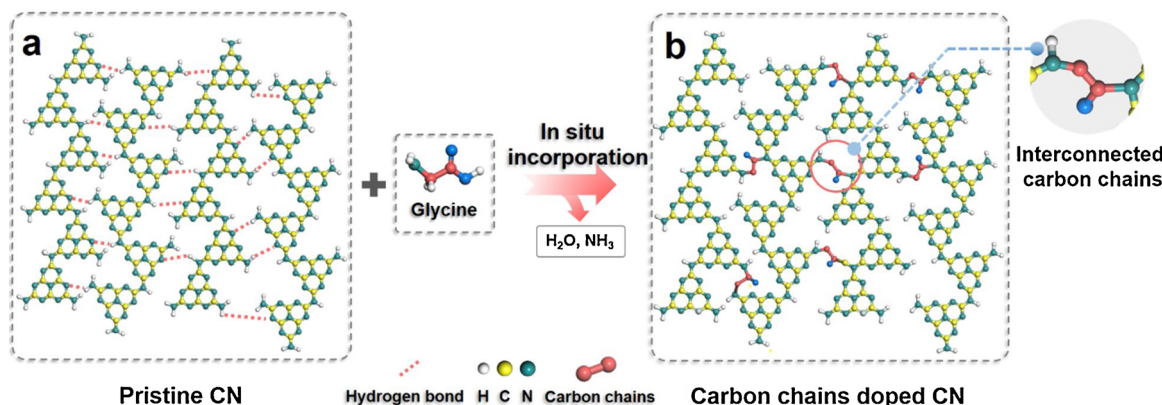
The photocatalytic H_2 evolution test was carried out in a glass reactor with a closed gas circulation system. The light source was a 300 W Xe lamp. 50 mg photocatalyst was firstly dispersed with a magnetic stirrer in triethanolamine aqueous solution (30 mL of triethanolamine and 220 mL of H₂O) and was loaded with 2 wt% Pt as the co-catalyst via a photodeposition process (under UV-vis light irradiation, $\lambda > 350$ nm). After Pt loading and vacuumizing, H_2 evolution over the photocatalyst was carried out under visible light irradiation (with an L42 filter, $\lambda > 400$ nm). The evolved H_2 was analyzed by online gas chromatography (GC-8A; Shimadzu Corp., Japan) equipped with a thermal conductivity detector.

2.4. Photocatalytic CO_2 reduction test

The photocatalytic CO_2 evolution test was carried out in a glass reactor with a closed gas circulation system. 20 mg photocatalyst, 1 μ mol CoCl₂, and 15 mg 2, 2-bipyridine were dispersed with a magnetic stirrer in solution (50 mL acetonitrile, 10 mL of H₂O and 2 mL of triethanolamine). After complete vacuumizing, the reaction system was injected with pure CO_2 (~80 kPa). The produced gases were analyzed by a gas chromatography. The light source was a 300 W Xe lamp (with a L42 cutoff filter and water filter, $\lambda > 400$ nm). The water filter used here is to remove the IR irradiation.

2.5. Photoelectrochemical measurement

The photoelectrodes were prepared according to previously reported method. The indium doped tin oxide (ITO) substrates were cleaned by ultrasonication in distilled water, absolute ethanol, and isopropanol for 15 min sequentially, and then dried in vacuum. 5 mg of photocatalysts and 20 μ L of Nafion solution (5 wt%) were dispersed in 1 mL ethanol by at least 30 min sonication to prepare a homogeneous catalyst colloid. Then, 100 μ L of the catalyst colloid was deposited onto areas of ≈ 1 cm² of the ITO conductive glass and then was dried in air to form the working electrode. The photoelectrochemical properties were investigated in a three-electrode cell by using an electrochemical station (Model-660D, CH instruments). The catalyst coated ITO glass, a Pt foil, and an Ag/AgCl electrode and 0.5 M Na₂SO₄ aqueous solution were used as the working electrode, the counter-electrode, the reference electrode, and the electrolyte, respectively. A 300 W Xe arc lamp equipped with a 400 nm cutoff filter was utilized as a light source. EIS were recorded at an applied potential of 0.2 V versus Ag/AgCl over the



Scheme 1. Structure of CN before a) and after b) doping with carbon chains. In the doping process, the glycine molecules were involved in the reaction with terminal groups, i.e., NH_2 and NH , in CN, and thus the carbon chains were interconnected with the tri-s-triazine units via $\text{C}-\text{N}$ bonds.

frequency range of 1 MHz–0.1 Hz. The photocurrent with on/off cycles was measured at an applied potential of 1.0 V versus Ag/AgCl. Mott–Schottky plots were obtained under direct current potential polarization at the frequency of 1000 Hz. The potential ranged from –0.6 to 1.0 V (vs Ag/AgCl).

3. Results and discussion

3.1. Atomic carbon chains linked polymeric CN

Generally, the key step for the generation of CN is the deamination process between amino groups of the precursors and intermediates. [28] Thus, these amino groups also possess the potential to react with NH_2 group or COOH group by releasing NH_3 and H_2O at some specified conditions, resulting in the formation of $\text{C}-\text{N}$ bonds. Inspired by this point, the glycine molecules, with terminated COOH and NH_2 groups and short length, are selected as the potential linker to bridge the in-plane defects of layered CN as illustrated in **Scheme 1**. The carbon chains linked CN was prepared by a direct thermal polymerization of melamine and glycine precursor and the obtained samples were denoted as CN-xGly (x means the amount of glycine). We use the glycine as a representative molecule to explore the underlying structure and performance of the products derived from melamine and glycine.

In situ FT-IR was conducted under Ar atmosphere to visualize the incorporating process of carbon chains, in which the detected signal at 100 °C was used as the background (**Fig. 1a**). The direct polymerization of melamine and glycine is quite a complicated process, wherein abundant old bonds break and new bonds form. To avoid the appearance of various FT-IR signals caused by the transformation of rich bonds and study the potential inserting process of small molecules in the framework of CN clearly, we loaded glycine molecules on stable pristine CN and employed this composite as the model for in situ FT-IR observation. The calcination-time dependent infrared spectra (**Fig. 1a**) present three distinct change regions. The signals in regions I and II increased gradually between 150–250 °C, whereas those in region III declined. When further increased the temperature up to 450 °C, all typical signals keep unchanged, indicating that glycine and CN could react entirely at approximately 250 °C and the established structure is steady even at high temperature. Here, we analyze the spectrum at 450 °C in detail to approach the established structure (**Fig. 1b**). The decreased absorbance at 3450 cm^{-1} can be ascribed to the consumption of NH_2 group, along with the newly appeared NH (3180 cm^{-1}), $\text{C}-\text{N}$ (1038 cm^{-1}) species, [29–31] suggesting that the suspended NH_2 groups adjacent to the tri-s-triazine units involved in the reaction with glycine and subsequently generated the $\text{C}-\text{NH}$ motif by releasing NH_3 molecules (marked with gray circle in **Fig. 1c**). The new bands at 1119 cm^{-1} ($\text{C}-\text{N}$) and 1656 cm^{-1} ($\text{C}=\text{O}$) imply the generation of $\text{N}-\text{C}=\text{O}$ species (marked with cyan circle in **Fig. 1c**) [4], which

stemmed from the dehydration reaction between the (C2)-NH motif of CN and the terminal COOH groups of glycine molecules. According to the newly formed $\text{C}-\text{N}$ and $\text{N}-\text{C}=\text{O}$ structural motifs, the structure schemed in **Fig. 1c** is proposed. Meanwhile, another similar moiety $\text{NH}-\text{C}=\text{O}$ (marked with red circle in **Fig. 1d**), obtained from the dehydration reaction between the NH_2 over CN and the COOH group of glycine molecule, also formed as identified by the bands located at 1338 cm^{-1} and 1531 cm^{-1} (reason for the different band position of $\text{N}-\text{C}=\text{O}$ and $\text{NH}-\text{C}=\text{O}$ motifs provided in SI-Discussion-1). For comparison, the different signals of pure CN and the glycine loaded Al_2O_3 from that of glycine loaded CN under same conditions further confirm that the glycine molecule chains indeed inserted into the framework of CN in the demonstrated way (**Fig. S1** and SI-Discussion-2). In brief, the analyses above identify that the carbon chains are indeed inserted into the defect of CN (**Scheme 1b**) and exist as two forms as illustrated in **Fig. 1c,d**.

The chemical structure and local electronic configuration of the CN with and without carbon chains were further examined by the synchrotron-based X-ray absorption spectroscopy (XAS) and X-ray photo-electron spectroscopy (XPS). The carbon K-edge XA spectra (**Fig. 1e**) present characteristic resonances of samples including π^* transitions in $\text{C}=\text{C}$ at 284.7 eV, $\text{N}=\text{C}-\text{N}$ at 287.5 eV and σ^* transitions in $\text{C}-\text{C}$ between 290 and 298 eV [32]. The intensity ratio of σ^* transition (in $\text{C}-\text{C}$) to π^* transitions (in $\text{N}=\text{C}-\text{N}$) of CN-10Gly was higher than that of pristine CN, which could be ascribed to the additional $\text{C}-\text{C}$ species from the doped carbon chains. (Note: $\text{N}=\text{C}-\text{N}$ is the inherent motif in CN, thus it can be regarded as the reference for the qualitative study of the induced foreign units.) In the nitrogen K-edge region (**Fig. 1f**), typical π^* resonances at 399.6 and 402.3 eV are observed, corresponding to aromatic nitrogen atoms of heterocyclic rings ($\pi^*_{\text{C}=\text{N}-\text{C}}$) and $\text{sp}^3 \text{N}-\text{C}$ bridging among tri-s-triazine moieties, respectively [32,33]. The 1 s \rightarrow $\sigma^*_{\text{N}-\text{C}}$ transition is located in the range of 404 to 412 eV [33,34]. Taking the intensity of intrinsic $\pi^*_{\text{C}=\text{N}-\text{C}}$ as reference, the CN-10Gly sample delivered higher intensity of $\sigma^*_{\text{N}-\text{C}}$ relative to that of CN, suggesting a slightly higher content of $\text{C}-\text{N}$ bonds in the carbon chains doped CN. It reveals how the carbon chains link with the matrix of CN, i.e., via covalent bonds between C and N as illustrated in **Fig. 1c,d**. The C and N K-edges XA spectra (Figs. S2a and S2b) of CN-10Gly-(two steps) (synthesis details provided in experimental section) show similar results with those of CN-10Gly, identifying the rationality of the adopted model, i.e., glycine molecules loaded unmodified CN, used in situ FT-IR examination. The high-resolution C 1 s XPS spectra (**Fig. 1g**) for pristine CN can be deconvoluted into two components located at 288.25 eV and 284.78 eV, assigned to $\text{N}-\text{C}=\text{N}$ motifs and adventitious hydrocarbons (in the form of $\text{C}-\text{C}$ or $\text{C}=\text{C}$), respectively. It was reported that the glycine loaded on graphene oxide showed a close binding energy at 284.6 eV, corresponding to the $\text{C}-\text{C}/\text{C}-\text{H}$ species in glycine [35]. Hence, the peak of designed carbon chains could overlap with the

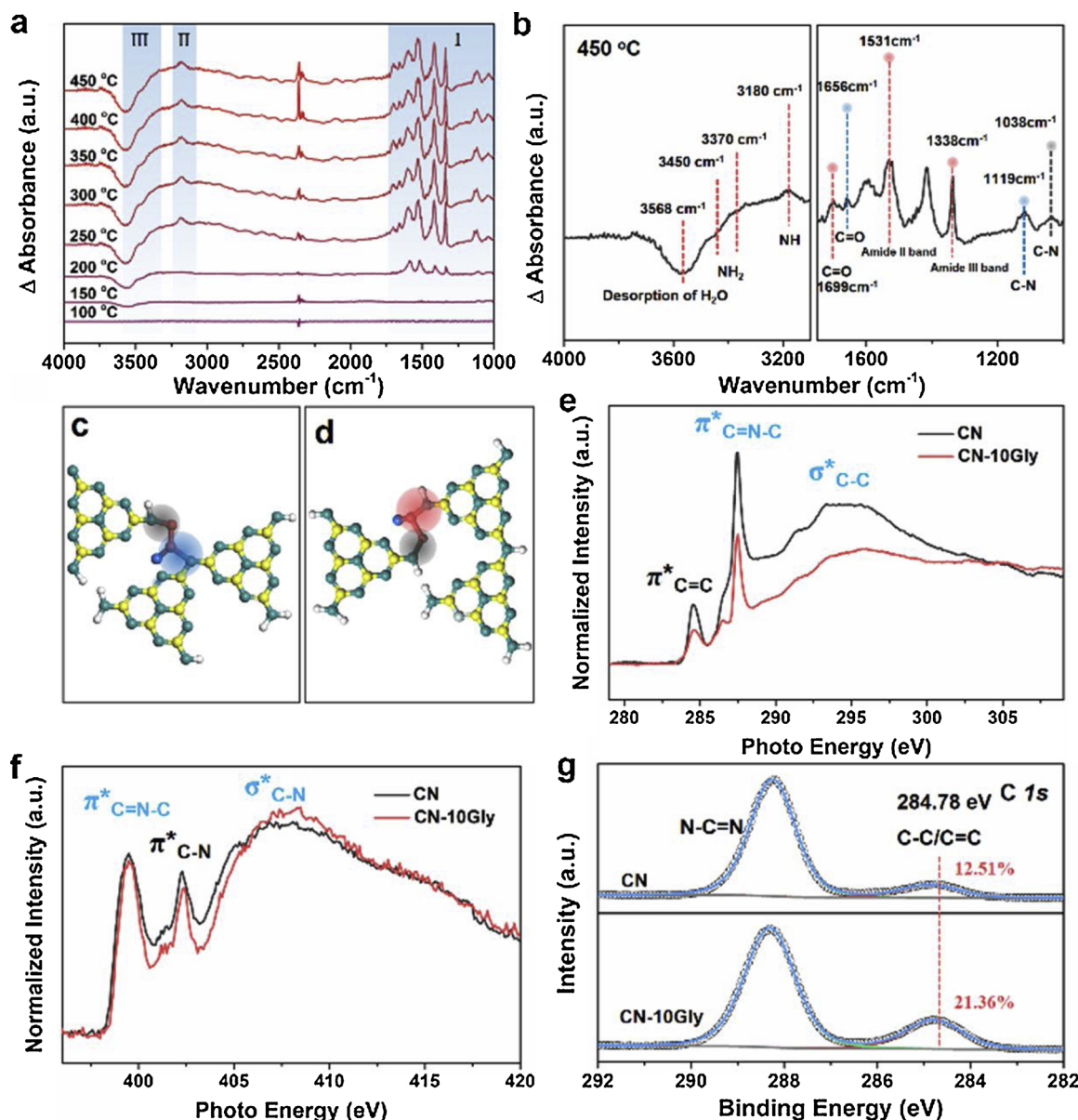


Fig. 1. Structure identification of the carbon chains incorporated CN. a) In situ FT-IR spectra of glycine loaded CN measured at different temperature. b) The in situ FT-IR spectrum at 450 °C. c,d) The illustration of two possible kinds of structure in the carbon chains doped CN. e,f) Carbon and nitrogen K-edge XA spectra of CN and CN-10Gly, respectively. g) The C 1s spectra of CN and CN-10Gly.

adventitious hydrocarbons due to the similar binding energy. Upon introducing the glycine into the feedstock (CN-10Gly), the percentage of C—C/C=C species to all detected carbon increased from 12.5% to 21.4% (Fig. 1g and Table S1), clearly suggesting that additional C—C chains contained in the CN-10Gly sample. The slightly increased atomic percentage of C and O (derived from XPS) in CN-10Gly relative to that of CN (Table S2) as well as the appearance of C=O species (Fig. S3), also discloses the successful incorporation of carbon chains in the CN.

The incorporation of carbon chains in CN was further verified by the UV-vis spectra, common-used FT-IR, solid-state NMR and high-resolution N 1s spectra (Fig. S4–S7; details provided in SI-Discussion-3). Apart from the reactive groups, i.e., COOH and NH₂, on the molecule chains, the match of dimension between the inserting molecules and defects of CN could be another critical factor that determines the incorporation of carbon chains into layers of CN. It's preliminarily identified that the size of inserted carbon chains is comparable to that of defects of CN according to the XRD analysis (Fig. S8a,b and SI-Discussion-4). Based on the above analyses, the carbon chains were

successfully planted in the basal plane of CN and connected the tri-s-triazine units through strong C—N bonds.

3.2. Carbon chains-mediated photocarriers separation and transport

The modified CN with carbon chains remained comparable morphology and surface area to that of CN (Fig. S9 and S10), further illustrating that the carbon chains were embedded in the framework of CN in manner of molecular distribution as demonstrated above. Besides, the doped carbon chains barely affected the band structure (Fig. S11) including the band gap (Fig. S11a), flat-band potential (Fig. S11b) and valence band (Fig. S11c).

Usually, carbon materials, such as carbon nanotube, graphene, and even the doped carbon matrix in basal plane of CN, own excellent electrical conductivity. Therefore, we believe that the carbon chains with two C atoms interconnected with the intrinsic structure of CN covalently could enable the electron with faster mobility throughout the layers compared with the original layers full of hydrogen bonds.

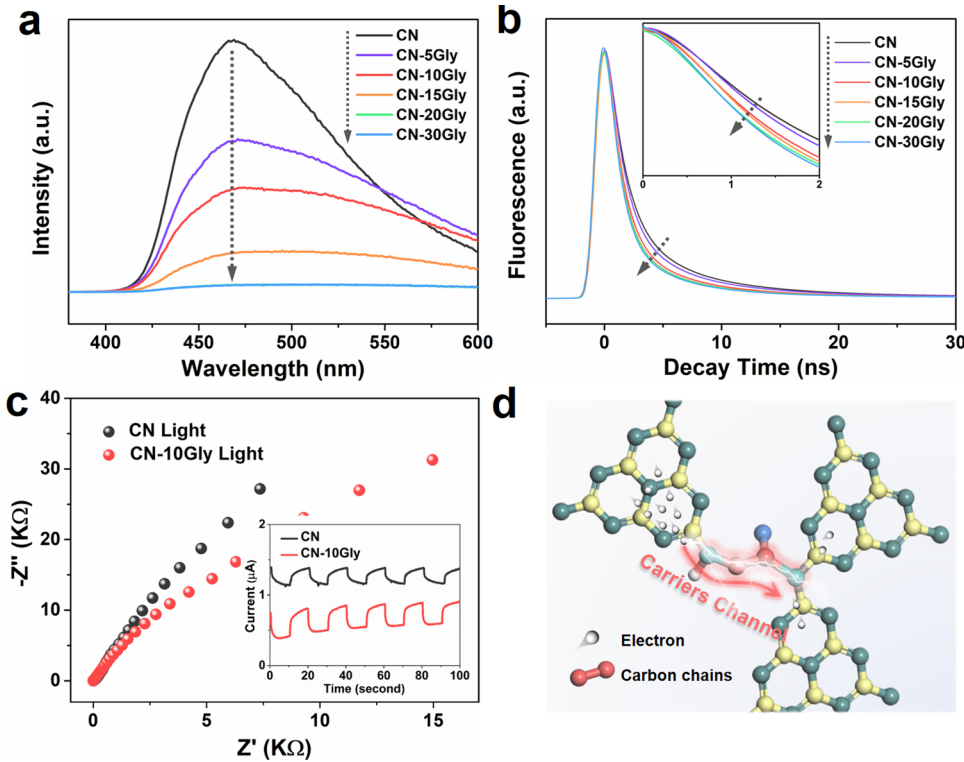


Fig. 2. Characterization of the photocarriers kinetics of the as-prepared samples. a,b) Steady-state and time-resolved photoluminescence spectroscopy of the samples, respectively. c) Electrochemical impedance spectroscopy (EIS) Nyquist plots under irradiation condition. Inset: Periodic on/off photocurrent response under visible-light irradiation. d) Schematic diagram of carriers channel role of bridged carbon chains.

Hence, we focus on the study related to the kinetics of photocarriers in the CN with and without carbon chains modification. Steady-state/time-resolved photoluminescence (PL) spectroscopy characterizations, as powerful tools to monitor the excitonic processes, i.e., radiative recombination of photogenerated electron-hole pairs in photocatalyst, were carried out for a series of samples. PL intensity represents the combination possibility of light-induced electron-hole pairs [36]. As shown in Fig. 2a, pristine CN gives a sharp emission peak at 470 nm, but the PL intensity is progressively and substantially suppressed with the increased incorporation amount of carbon chains. This phenomenon means greatly enhanced separation and transfer of photocarriers, as profited from promotional effect of the carbon chains. In particular, time-resolved PL spectra of the doped samples (Fig. 2b) detected at the emission wavelength, i.e., 470 nm, show the gradual and apparent decrease in fluorescence lifetime (fitted from the decay spectra, Table S3) in comparison with the unmodified CN. The fluorescence decay of the as-prepared samples is entirely in line with their decrease tendency of PL intensities, suggesting faster separation and transfer of electrons and holes in the framework of CN [6]. It signifies that the more photo-generated carriers captured by reactive substrates under reaction conditions, the more efficient photocatalysis reactions realized for carbon chains linked CN.

We also used photoelectrochemical characterizations to investigate the carriers separation and transfer behavior of as-prepared samples. Nyquist plot of CN-10Gly under the dark condition presents apparently declined semicircles in comparison with that of the pristine CN (Fig. S12), indicative of the more favorable inherent electron transport ability. Upon irradiation with visible light, both of them show decreased semicircles and the carbon chains modified sample still exhibits smaller resistance value compared to the pristine CN (Fig. 2c). Above results suggest a significantly improved electronic conductivity in the non-photoexcited and photoexcited status. Meanwhile, a marked enhancement of photocurrent (inset of Fig. 2c) is also observed for CN-10Gly relative to pristine CN, which further illustrates that the mobility of the photo-carriers is promoted remarkably. By combining the results as mentioned earlier, we can reasonably conclude that the embedded

carbon chains in the plane of CN can dramatically promote the separation and transfer of photocarriers within the framework of CN.

3.3. Superior light-driven H₂ evolution and CO₂ reduction

To assess the validity of carbon chains integration strategy over CN on improving photocatalytic efficiency, photocatalytic H₂ evolution was carried out over the as-synthesized samples. All the samples modified with various carbon chains (Fig. 3a) exhibit substantial improvement in photocatalytic H₂ evolution in contrast to pristine CN. Particularly, CN-10Gly presents the highest H₂ evolution activity, increased by 13.2 times in comparison with that of pristine CN. Our strategy is not only quite simple but also achieves a high activity, i.e., among the top records for the in-plane engineered CN in H₂ evolution (Table S4). This modification strategy also dramatically boosts the photocatalytic CO₂ reduction performance because more photoelectrons are available for reactants at the interface between photocatalyst and reaction solution. The optimized sample (CN-10Gly) exhibits a 29.2 times enhancement relative to CN in CO generation (Fig. 3b). Both the gaseous products for water splitting and CO₂ reduction over the optimized sample increased linearly with the irradiation time (Fig. S13), suggesting good stability for CN-10Gly. It is further evidenced by the long-term H₂ evolution as shown in Fig. 3c, only a slight decrease was observed during the 20 h test. An adverse effect emerged for both H₂ evolution (Fig. 3a) and CO evolution (Fig. 3b) when excessive glycine was introduced. Actually, a similar phenomenon has also been revealed in the relevant studies [37,38]. The negative effect could be ascribed to the fact that introducing too many foreign units may inevitably destruct the conjugated structures of CN [37,38]. As a result, it could diminish the positive effect of efficient separation of photocarriers, leading to a decline in photocatalytic activity. Interestingly, when maintaining the terminal groups as COOH and NH₂ but increasing the carbon atom number in the doping molecule from two to four, the activity of samples presents a drastic change (Fig. S14). When the carbon number is three, the H₂ evolution rate, reaching up to ~167 μmol/h, is almost twice that of glycine (carbon number is equal to two) modified sample (90 μmol/h).

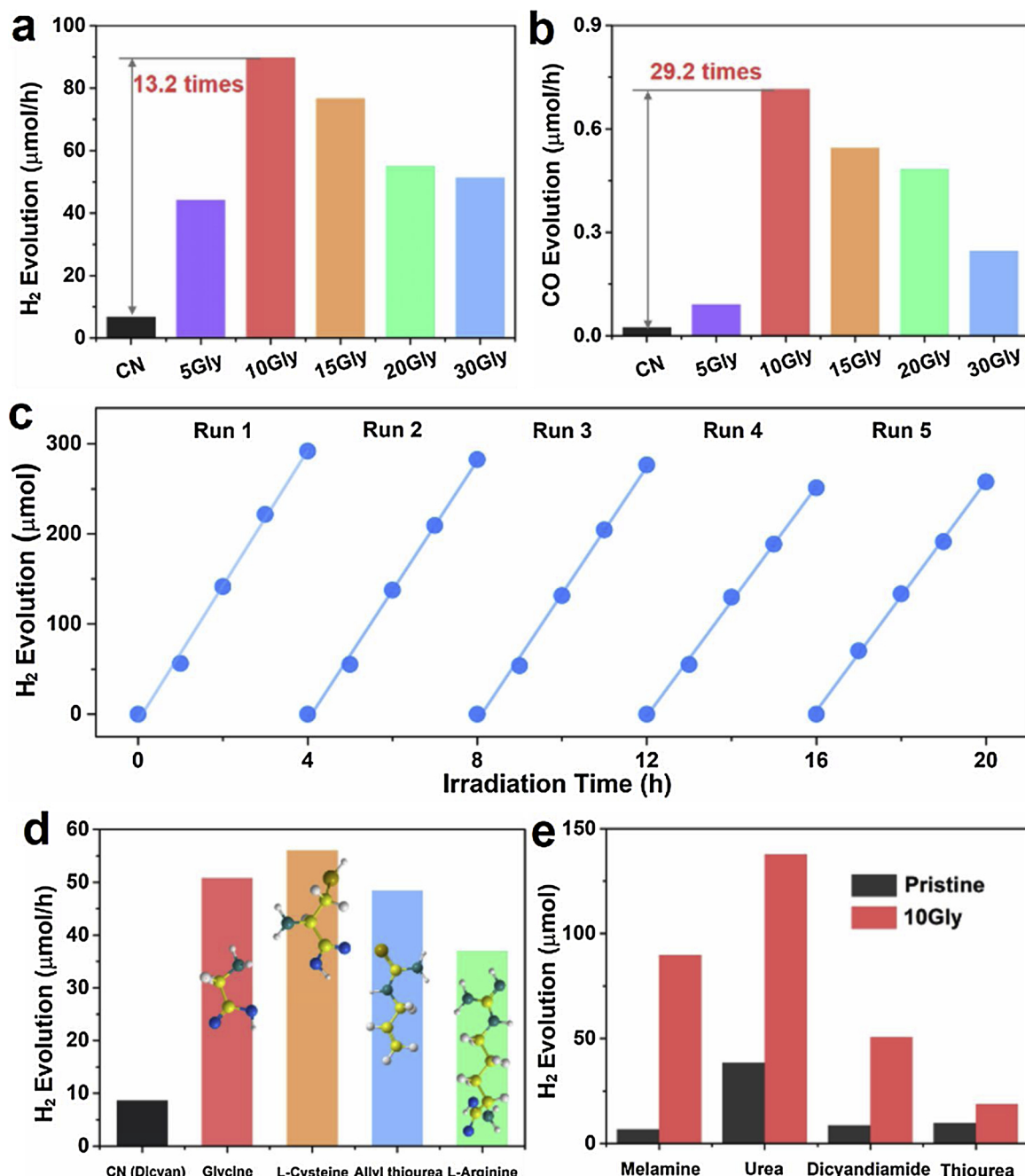


Fig. 3. Photocatalytic activity evaluation of the as-prepared samples. a,b) Comparison of the photocatalytic H₂ evolution and CO₂ reduction rate of the samples with different amount of glycine, respectively. c) Cycle test of H₂ evolution over CN-10Gly. d) Comparison of the photocatalytic H₂ evolution activity of samples obtained from dicyandiamide and different kinds of small molecules. e) Comparison of the photocatalytic H₂ evolution activity of samples derived from glycine and different precursors.

h) and 24.6 folds higher than pristine CN. However, the activity (23 μmol/h) decreases drastically as the carbon number further increased to four. We preliminarily ascribe this phenomenon to the match degree of size between defects and molecules, that is, the dimension of molecules containing two or three carbon atoms is comparable to that of defects; however, the molecules with four carbon atoms are hard to be embedded into the defects of CN. Further studies are still needed to validate this assumption.

To further demonstrate the universality of this strategy, various precursors and molecule linkers (Fig. S15) have been adopted. All the as-prepared samples (Fig. 3d,e) exhibited significant enhancement in H₂ evolution. (Note: these molecule chains linkers, i.e., L-cysteine, Allyl thiourea and L-Arginine, possess groups on adjacent C atoms, including

NH, NH₂ and COOH groups, which are apt to react with the residual NH₂ or NH groups in CN.)

4. Conclusions

In conclusion, our study demonstrates a facile and efficient strategy to incorporate short carbon chains into the basal plane of CN while remaining the pristine tri-s-triazine structure. The carbon chains filled the defects in CN via covalent bonds, which mediates the electron transfer in a relatively smooth transport channel compared to the initial hydrogen bonds. By virtue of such a favorable transport channel of carriers, the carbon chains linked CN exhibits a dramatically improved photocatalytic water splitting and CO₂ reduction performance,

achieving a 13.2 and 29.2 times enhancement, respectively, compared to pristine CN. This study highlights that the engineering of the defects in photocatalysts is one of the most effective approaches for improving solar energy conversion and also gives a research direction for the future rational design towards efficient photocatalysts, especially for organic-based ones.

Acknowledgements

This work received financial support from the World Premier International Research Center Initiative (WPI Initiative) on Materials Nanoarchitectonics (MANA), MEXT (Japan), JSPS KAKENHI (JP18H02065), the Photo-excitonix Project at Hokkaido University, National Natural Science Foundation of China (21633004).

Appendix A. Supplementary data

Supplementary material related to this article can be found, in the online version, at doi:<https://doi.org/10.1016/j.apcatb.2019.118027>.

References

- [1] S.N. Habisreutinger, L. Schmidt-Mende, J.K. Stolarczyk, Photocatalytic reduction of CO₂ on TiO₂ and other semiconductors, *Angew Chem Int Ed* 52 (2013) 7372–7408.
- [2] X. Wang, K. Maeda, A. Thomas, K. Takanabe, G. Xin, J.M. Carlsson, K. Domen, M. Antonietti, A metal-free polymeric photocatalyst for hydrogen production from water under visible light, *Nat. Mater.* 8 (2009) 76–80.
- [3] G. Zhang, G. Li, T. Heil, S. Zafeiratos, A. Savateev, X. Wang, M. Antonietti, Tailoring grain boundary chemistry of polymeric carbon nitride for enhanced solar H₂ production and CO₂ reduction, *Angew. Chem. Int. Ed.* 58 (2019) 3433–3437.
- [4] G. Zhao, H. Pang, G. Liu, P. Li, H. Liu, H. Zhang, L. Shi, J. Ye, Co-porphyrin/carbon nitride hybrids for improved photocatalytic CO₂ reduction under visible light, *Appl. Catal. B* 200 (2017) 141–149.
- [5] P. Yang, H. Zhuzhang, R. Wang, W. Lin, X. Wang, Carbon vacancies in a melon polymeric matrix promote photocatalytic carbon dioxide conversion, *Angew. Chem. Int. Ed. Engl.* 58 (2019) 1134–1137.
- [6] Y. Li, S. Ouyang, H. Xu, X. Wang, Y. Bi, Y. Zhang, J. Ye, Constructing Solid-Gas-Interfacial Fenton reaction over Alkalized-C₃N₄ photocatalyst to achieve apparent quantum yield of 49% at 420 nm, *J. Am. Chem. Soc.* 138 (2016) 13289–13297.
- [7] N. Tian, K. Xiao, Y. Zhang, X. Lu, L. Ye, P. Gao, T. Ma, H. Huang, Reactive sites rich porous tubular yolk-shell g-C₃N₄ via precursor recrystallization mediated microstructure engineering for photoreduction, *Appl. Catal. B* 253 (2019) 196–205.
- [8] J. Cai, J. Huang, S. Wang, J. Iocozzia, Z. Sun, J. Sun, Y. Yang, Y. Lai, Z. Lin, Crafting mussel-inspired metal nanoparticle-decorated ultrathin graphitic carbon nitride for the degradation of chemical pollutants and production of chemical resources, *Adv. Mater.* 31 (2019) e1806314.
- [9] G. Liao, Y. Gong, L. Zhang, H. Gao, G.-J. Yang, B. Fang, Semiconductor polymeric graphitic carbon nitride photocatalysts: the “holy grail” for the photocatalytic hydrogen evolution reaction under visible light, *Energy Environ. Sci.* 12 (2019) 2080–2147.
- [10] W. Cui, J. Li, Y. Sun, H. Wang, G. Jiang, S.C. Lee, F. Dong, Enhancing ROS generation and suppressing toxic intermediate production in photocatalytic NO oxidation on O/Ba co-functionalized amorphous carbon nitride, *Appl. Catal. B* 237 (2018) 938–946.
- [11] J. Cheng, Z. Hu, K. Lv, X. Wu, Q. Li, Y. Li, X. Li, J. Sun, Drastic promoting the visible photoreactivity of layered carbon nitride by polymerization of dicyandiamide at high pressure, *Appl. Catal. B* 232 (2018) 330–339.
- [12] J. Ji, J. Wen, Y. Shen, Y. Lv, Y. Chen, S. Liu, H. Ma, Y. Zhang, Simultaneous non-covalent modification and exfoliation of 2D carbon nitride for enhanced electrochemiluminescent biosensing, *J. Am. Chem. Soc.* 139 (2017) 11698–11701.
- [13] J. Li, D. Wu, J. Iocozzia, H. Du, X. Liu, Y. Yuan, W. Zhou, Z. Li, Z. Xue, Z. Lin, Achieving efficient incorporation of π-electrons into graphitic carbon nitride for markedly improved hydrogen generation, *Angew. Chem.* 58 (2019) 1985–1989.
- [14] Z. Teng, N. Yang, H. Lv, S. Wang, M. Hu, C. Wang, D. Wang, G. Wang, Edge-functionalized g-C₃N₄ nanosheets as a highly efficient metal-free photocatalyst for safe drinking water, *Chem* 5 (2019) 664–680.
- [15] H. Yu, L. Shang, T. Bian, R. Shi, G.I. Waterhouse, Y. Zhao, C. Zhou, L.Z. Wu, C.H. Tung, T. Zhang, Nitrogen-doped porous carbon nanosheets templated from g-C₃N₄ as metal-free electrocatalysts for efficient oxygen reduction reaction, *Adv. Mater.* 28 (2016) 5080–5086.
- [16] Z. Chen, E. Vorobyeva, S. Mitchell, E. Fako, M.A. Ortúñoz, N. López, S.M. Collins, P.A. Midgley, S. Richard, G. Vilé, J. Pérez-Ramírez, A heterogeneous single-atom palladium catalyst surpassing homogeneous systems for Suzuki coupling, *Nat. Nanotechnol.* 13 (2018) 702–707.
- [17] P. Yang, L. Wang, H. Zhuzhang, R. Wang, M.-M. Titirici, X. Wang, Photocarving nitrogen vacancies in a polymeric carbon nitride for metal-free oxygen synthesis, *Appl. Catal. B* 256 (2019) 117794.
- [18] Y. Li, H. Xu, S. Ouyang, D. Lu, X. Wang, D. Wang, J. Ye, In situ surface alkalinated g-C₃N₄ toward enhancement of photocatalytic H₂ evolution under visible-light irradiation, *J. Mater. Chem. A* 4 (2016) 2943–2950.
- [19] Y. Zheng, J. Liu, J. Liang, M. Jaroniec, S.Z. Qiao, Graphitic carbon nitride materials: controllable synthesis and applications in fuel cells and photocatalysis, *Energy Environ. Sci.* 5 (2012) 6717–6731.
- [20] P. Qiu, C. Xu, N. Zhou, H. Chen, F. Jiang, Metal-free black phosphorus nanosheets-decorated graphitic carbon nitride nanosheets with C–P bonds for excellent photocatalytic nitrogen fixation, *Appl. Catal. B* 221 (2018) 27–35.
- [21] J. Cheng, Z. Hu, Q. Li, X. Li, S. Fang, X. Wu, M. Li, Y. Ding, B. Liu, C. Yang, L. Wen, Y. Liu, K. Lv, Fabrication of high photoreactive carbon nitride nanosheets by polymerization of amidinourea for hydrogen production, *Appl. Catal. B* 245 (2019) 197–206.
- [22] Y. Kang, Y. Yang, L.C. Yin, X. Kang, L. Wang, G. Liu, H.M. Cheng, Selective breaking of hydrogen bonds of layered carbon nitride for visible light photocatalysis, *Adv. Mater.* 28 (2016) 6471–6477.
- [23] B.V. Lotsch, M. Döblinger, J. Sehnert, L. Seyfarth, J. Senker, O. Oeckler, W. Schnick, Unmasking melon by a complementary approach employing Electron diffraction, solid-state NMR spectroscopy, and theoretical calculations—structural characterization of a carbon nitride polymer, *Chem. – Eur. J.* 13 (2007) 4969–4980.
- [24] L. Lin, H. Ou, Y. Zhang, X. Wang, Tri-s-triazine-Based Crystalline Graphitic Carbon Nitrides for Highly Efficient Hydrogen Evolution Photocatalysis, *ACS Catal.* 6 (2016) 3921–3931.
- [25] W. Che, W. Cheng, T. Yao, F. Tang, W. Liu, H. Su, Y. Huang, Q. Liu, J. Liu, F. Hu, Z. Pan, Z. Sun, S. Wei, Fast photoelectron transfer in (Cring)-C₃N₄ plane heterostructural nanosheets for overall water splitting, *J. Am. Chem. Soc.* 139 (2017) 3021–3026.
- [26] Y. Yu, W. Yan, X. Wang, P. Li, W. Gao, H. Zou, S. Wu, K. Ding, Surface engineering for extremely enhanced charge separation and photocatalytic hydrogen evolution on g-C₃N₄, *Adv. Mater.* 30 (2018) 1705060.
- [27] Y. Wang, X. Liu, J. Liu, B. Han, X. Hu, F. Yang, Z. Xu, Y. Li, S. Jia, Z. Li, Y. Zhao, Carbon quantum dot implanted graphite carbon nitride nanotubes: excellent charge separation and enhanced photocatalytic hydrogen evolution, *Angew. Chem. Int. Ed.* 57 (2018) 5765–5771.
- [28] A. Thomas, A. Fischer, F. Goettmann, M. Antonietti, J.-O. Müller, R. Schlögl, J.M. Carlsson, Graphitic carbon nitride materials: variation of structure and morphology and their use as metal-free catalysts, *J. Mater. Chem.* 18 (2008) 4893–4908.
- [29] G. Zhao, Y. Sun, W. Zhou, X. Wang, K. Chang, G. Liu, H. Liu, T. Kako, J. Ye, Superior photocatalytic H₂ production with cocatalytic Co/Ni species anchored on sulfide semiconductor, *Adv. Mater.* 29 (2017) 1703258.
- [30] H. Yu, R. Shi, Y. Zhao, T. Bian, Y. Zhao, C. Zhou, G.I.N. Waterhouse, L.Z. Wu, C.H. Tung, T. Zhang, Alkali-assisted synthesis of nitrogen deficient graphitic carbon nitride with tunable band structures for efficient visible-light-Driven hydrogen evolution, *Adv. Mater.* 29 (2017) 1605148–1605154.
- [31] P. Niu, L. Zhang, G. Liu, H.-M. Cheng, Graphene-like carbon nitride nanosheets for improved photocatalytic activities, *Adv. Funct. Mater.* 22 (2012) 4763–4770.
- [32] Y. Zheng, Y. Jiao, Y. Zhu, L.H. Li, Y. Han, Y. Chen, A. Du, M. Jaroniec, S.Z. Qiao, Hydrogen evolution by a metal-free electrocatalyst, *Nat. Commun.* 5 (2014) 3783.
- [33] N. Meng, J. Ren, Y. Liu, Y. Huang, T. Petit, B. Zhang, Engineering oxygen-containing and amino groups into two-dimensional atomically-thin porous polymeric carbon nitrogen for enhanced photocatalytic hydrogen production, *Energy Environ. Sci.* 11 (2018) 566–571.
- [34] H.B. Yang, J. Miao, S.F. Hung, J. Chen, H.B. Tao, X. Wang, L. Zhang, R. Chen, J. Gao, H.M. Chen, L. Dai, B. Liu, Identification of catalytic sites for oxygen reduction and oxygen evolution in N-doped graphene materials: development of highly efficient metal-free bifunctional electrocatalyst, *Sci. Adv.* 2 (2016) e1501122.
- [35] K. Pytlakowska, V. Kozik, M. Matussek, M. Pilch, B. Hachula, K. Kocot, Glycine modified graphene oxide as a novel sorbent for preconcentration of chromium, copper, and zinc ions from water samples prior to energy dispersive X-ray fluorescence spectrometric determination, *RSC Adv.* 6 (2016) 42836–42844.
- [36] D. Zheng, X.N. Cao, X. Wang, Precise formation of a hollow carbon nitride structure with a Janus surface to promote water splitting by photoredox catalysis, *Angew. Chem. Int. Ed.* 55 (2016) 11512–11516.
- [37] J. Zhang, G. Zhang, X. Chen, S. Lin, L. Mohlmann, G. Dolega, G. Lipner, M. Antonietti, S. Blechert, X. Wang, Co-monomer control of carbon nitride semiconductors to optimize hydrogen evolution with visible light, *Angew. Chem. Int. Ed.* 51 (2012) 3183–3187.
- [38] J. Qin, S. Wang, H. Ren, Y. Hou, X. Wang, Photocatalytic reduction of CO₂ by graphitic carbon nitride polymers derived from urea and barbituric acid, *Appl. Catal. B* 179 (2015) 1–8.